Flexural Stiffness of MAPP-Coupled PP–Henequen Composites: Micromechanical Modeling of Structure–Property Relationships

Faust Seculi ,* Francesc X. Espinach , Manel Alcalà , and Joan Ximinis

The flexural behavior and intrinsic mechanical properties were studied for polypropylene (PP) composites reinforced with 20 to 50 wt.% henequen strands, using maleic anhydride grafted polypropylene (MAPP) as compatibilizer. The maximum strain at break of the fibers was estimated by regression-based extrapolation (ε = 8%), which enabled calculation of the microfibrillar angle (MFA = 22.8°) using a modified Satyanarayana approach. Together with cellulose content and crystallinity, the resulting structural parameter (δ = 1.72) confirmed the suitability of henequen strands as reinforcement for thermoplastic composites. The composite flexural modulus exhibited a linear increase with fiber volume fraction (R^2 = 0.99), rising from 1.15 GPa for neat PP to 3.75 GPa at 50 wt.% fiber content, while the strain at break decreased consistently with increasing reinforcement content. Predictions obtained using the Hirsch model and the modified rule of mixtures, with efficiency factors (η_e) ranging from 0.45 to 0.55, showed good agreement with experimental results. Furthermore, three micromechanical models, Hirsch, Tsai–Pagano, and Nielsen, yielded consistent intrinsic flexural moduli for the henequen strands, in the range of 16 to 17 GPa. These results highlight the reinforcing potential of henequen strands and reveal their effectiveness in increasing the flexural stiffness of polypropylene-based composites.

DOI: 10.15376/biores.21.3.8226-8248

Keywords: Henequen; Polypropylene composites; Flexural modulus; Natural fiber reinforcement; Micromechanical modeling

*Contact information: LEPAMAP-PRODIS Research Group, University of Girona, 17003 Girona, Spain; * Corresponding author: faust.seculi@udg.edu*

INTRODUCTION

The progressive depletion of oil-based polymers is a priority given their life-cycle burdens, including substantial greenhouse gas emissions and fossil carbon use, limited circularity, and the persistence of macro- and microplastics in the environment (Geyer *et al.* 2017; Zheng and Suh 2019; Meys *et al.* 2021; Piao *et al.* 2024). These concerns are amplified by rising production volumes and constrained end-of-life performance in current systems, especially in packaging-intensive applications (Geyer *et al.* 2017; Plastics Europe 2024).

Within this context, substituting a fraction of polymers with natural fiber-reinforced polymers (NFRPs) offers an incremental route to lower embodied carbon and mass while retaining structural utility (Maurya and Manik 2023; Tran *et al.* 2025). NFRPs combine thermoplastic matrices with lignocellulosic fibers whose diversity in morphology, chemistry and, mechanical properties enable tailoring to performance and processing

windows (Joseph *et al.* 2002; Hariprasad *et al.* 2020; Erana 2024). Fully bio-based matrices continue to advance, yet industrial uptake remains uneven due to cost, thermal/processing compatibility, supply reliability, and qualification constraints; in parallel, NFRPs formulated with the most widely used thermoplastics (polyolefins, notably PP) have already penetrated established value chains (OECD 2024; Plastics Europe 2024).

Among plant fibers, henequen (*Agave fourcroydes*) is an attractive reinforcement for polypropylene (PP): it provides favorable specific stiffness (Serra-Parareda *et al.* 2021), a surface conducive to mechanical interlocking, and a renewable origin. Typically, henequen fibers present a cellulose content ranging from 60 to 78 wt.%, hemicellulose contents between 4 and 28 wt.%, lignin contents between 8 and 13 wt.%, and pectin contents around 3 to 4 wt.%. In addition, they present a density close to 1.49 g/cm^3 and diameters ranging from approximately 20 to 500 μm, depending on extraction and processing conditions (Biagiotti *et al.* 2004). Interfacial and flexural improvements have been obtained through surface treatments and interface engineering in PP–henequen systems (Cho *et al.* 2007; Lee *et al.* 2008), and recent PP/*Agave* composite reports highlight the stiffening potential in injection-moulded formulations and the sensitivity of performance to interface quality, even in related PE matrices (Anaya-Ramirez *et al.* 2022; Mansouri *et al.* 2024).

A central determinant of performance in NFRPs is the matrix–fiber interface. Lignocellulosic fibers are hydrophilic and heterogeneous; diameter, aspect ratio, the presence of a lumen, wall architecture and surface chemistry govern wetting, stress transfer, damage initiation and durability (Joseph *et al.* 2002; Hariprasad *et al.* 2020). Coupling agents are therefore critical: in PP systems, maleic anhydride-grafted polypropylene (MAPP) is widely used to promote interfacial bonding with fiber hydroxyl groups, enhancing load transfer and frequently increasing stiffness/strength of such composite materials (El-Sabbagh 2014; Anbupalani *et al.* 2020; Çavuş and Mengeloğlu 2020). Moreover, systematic studies show optimum MAPP/fiber ratios ~10 TO 13% relative to fiber mass (at 30 to 50 wt.% fiber)—equivalent to low single-digit wt.% on a composite basis—balancing adhesion against embrittlement and decreases in the material's processability (El-Sabbagh 2014).

This work focused on the flexural modulus of PP–henequen composites as a function of fiber content (20 to 50 wt.%), using a fixed 4 wt.% MAPP loading identified in prior PP–agave/henequen research and broader natural-fiber PP literature as near-optimal for increasing the interfacial adhesion without undue loss of toughness (El-Sabbagh 2014; Anaya-Ramirez *et al.* 2022; Mansouri *et al.* 2024). Flexural stiffness is a key selection metric for panels, housings, and semi-structural parts under bending and is sensitive to orientation, length efficiency and interface quality, thus serving as an informative probe of micromechanics (Joseph *et al.* 2002; Erana 2024).

The first aim of the study was to quantify the evolution of flexural modulus with fiber content under standardized testing, complementing available tensile/flexural datasets for PP–agave/henequen systems (Lee *et al.* 2008; Mansouri *et al.* 2024). The study interpreted stiffness trends using classical and semi-empirical models, rule-of-mixtures with orientation/length factors, Hirsch mixing, Halpin–Tsai/Pagano and Nielsen's modification (Cox 1952; Affdl and Kardos 1976; Nairn and Mendels 2001; Clyne and Hull 2019; Anbupalani *et al.* 2020). Finally, the intrinsic parameters (effective fiber modulus, interfacial/efficiency factors) were estimated by confronting experimental data with multiple models and cross-validating internal consistency. Comparative analyses in natural-fiber composites show Hirsch and Halpin–Tsai often bracket experimental moduli

for semi-random/short-fiber reinforced systems (Affdl and Kardos 1976; Chichane *et al.* 2023).

Collectively, the results provide a structure–property map for the PP–henequen strands–MAPP system that links fiber fraction, interface engineering and flexural stiffness, informing formulation choices for applications seeking to reduce oil-based content while maintaining stiffness-driven performance (Zheng and Suh 2019; Meys *et al.* 2021).

EXPERIMENTAL

Materials

The polymer matrix used for the fabrication of composite materials was homopolymer polypropylene (PP) of grade ISPLEN PP090 G2M, provided by Repsol Química, S.A. (Tarragona, Spain). This injection-grade PP (ISPLEN PP090 G2M) has a melt flow index of 30 g/10 min (at 230 °C with a 2.16 kg load) and a density of 0.905 g/cm³.

To increase the strength of the interface, maleic acid grafted polypropylene (MAPP) of grade Epolene G3015, acquired from Eastman Chemical Products (San Roque, Spain), and with an acid number of 15 mg KOH/g and a molecular weight of 24,800 Da, was employed.

The henequen strands (HS), used as reinforcement, were derived from *Agave fourcroydes* and procured from the Centro de Investigación Científica de Yucatán (CICY) in Mérida, Mexico. The strands contained 68.1% cellulose, 18.2% hemicellulose, 8.7% lignin, 3.7% extractives, and 1.3% ashes (Tarrés *et al.* 2019).

Fiber Characterization

X-ray diffraction (XRD) patterns were acquired using a PANalytical X′Pert PRO MPD diffractometer, equipped with a focusing mirror and operating in transmission mode. The instrument utilized Cu-Kα radiation (λ =1.542 Å) with an applied current of 40 mA.

To estimate the fiber's crystallinity index (CI), XRD was performed in reflection mode using the same diffractometer. The incident beam height was set to 0.4 mm, defined by the fixed divergence and anti- scatter slits. The CI was calculated using the Segal peak-height method according to Eq. 1 (Segal *et al.* 1959),

$$CI = \frac{I_{002} - I_{am}}{I_{002}} \quad (1)$$

where I_{002} corresponds to the maximum intensity of the (002) crystalline peak (around $2\theta \approx$ 22-23°), and I_{am} represents the intensity of the amorphous contribution (around $2\theta \approx$ 18°).

The analysis focused solely on quantifying the relative proportion of crystalline domains within the fiber structure, without deriving or interpreting any additional structural parameters. The resulting crystallinity index was used as a standalone metric to support subsequent discussions on fiber organization and its potential influence on composite performance.

Composite Materials Obtention

HS were chopped to lengths of 1 mm. Previous research on the same PP–henequen system showed that increasing the initial fiber length does not necessarily result in a

proportional increase in the effective fiber length after processing due to the attrition occurring during compounding (Serra-Parareda *et al.* 2021). The average diameter of the fibers was measured using optical microscopy, resulting in a value of 220.8 μm.

Composite materials were synthesized using a Brabender Plastograph mixer (Brabender®, Duisburg, Germany) featuring two counter-rotating screws to ensure optimal dispersion. Initially, PP and MAPP were simultaneously introduced into the mixing chamber, maintained at a temperature of 180 °C and a rotation speed of 80 rpm, until the mixture was fully molten. Subsequently, HS, were added while maintaining the same temperature and rotational speed. During this process, the fibers are subjected to attrition phenomena, and their length is reduced considerably. This impacts the aspect ratio of the reinforcements and its potential to strengthen and stiffen the composite materials.

The effective fiber dimensions used in the subsequent micromechanical analysis correspond to measurements previously reported (Espinach *et al.* 2022), obtained from the same set of composite specimens analyzed in the present study. In the cited paper, the intrinsic tensile strength of henequen-reinforced composites was evaluated using specimens from the same experimental batch analyzed in the present study. The only difference between the two works was the specimen geometry, which was intended for tensile testing in the former study and for flexural testing in the present one. Since both geometries are simultaneously produced using the same steel injection mold, no significant differences in the average fiber morphological properties are expected. Upon completion of the mixing process, the composite material was extricated from the chamber, allowed to cool, and then ground using a knife mill equipped with a 5 mm mesh screen at its base to ensure uniform granule size. The resulting granules were then stored at 80 °C for 24 h to eliminate any residual moisture.

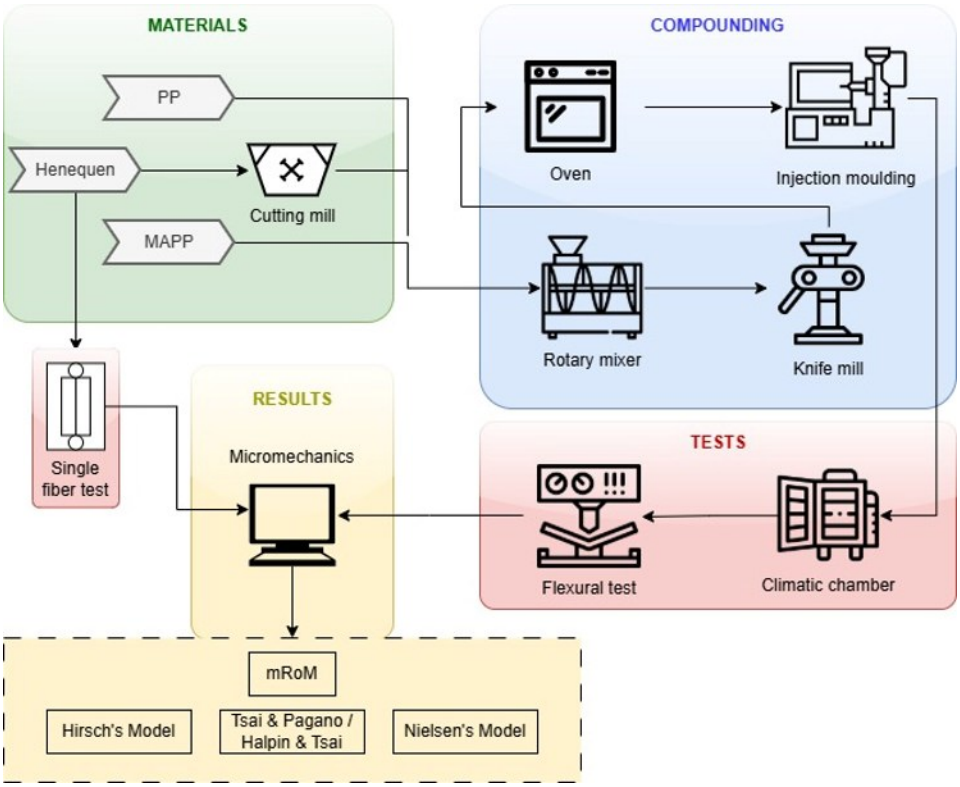

Fig. 1. Flowchart of the procedure: from raw materials processing to micromechanical modelling

A steel mold was used to fabricate samples in an injection molding machine Meteor-40 (Mateu and Solé, Spain). The injection molding process was conducted with the following temperature settings: 175 °C in zone 1, 175 °C in zone 2, and 190 °C at the nozzle, adhering to ASTM D3641 (2024) requirements for the three heating zones of the injection machine. Prior to flexural testing, the specimens were conditioned in a climate control chamber at 23 °C and 50% relative humidity for 48 h, following ASTM D618-21 (2021) standards. Flexural properties were measured using a universal testing machine (INSTRON 1122) operating at a crosshead speed of 2 mm/min, in accordance with ASTM D790-17 (2026) specifications.

Single-fiber Test

Single-fiber tensile tests were conducted in accordance with ASTM D3822-01 (2017) (Fig. 2). Individual fibers were randomly selected and mounted one-by-one onto a Minimat-type cardboard frame featuring identical rectangular windows. Tests were performed using a 200 N load cell: one end of the frame was secured in a stationary grip, while the opposite end was clamped in a moving grip operating at a constant crosshead speed. The applied force was recorded continuously as the fiber was loaded in tension to failure. The crosshead speed was set to 0.635 mm s^{-1}, corresponding to 10% of the calibrated gauge length, to ensure a strain at break below 8%.

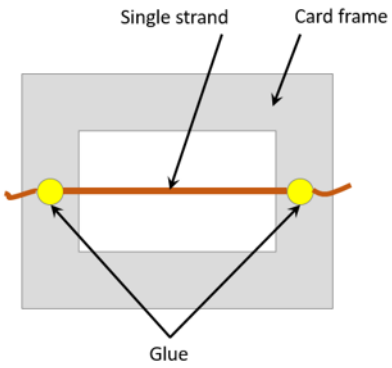

Fig. 2. Representation of the single fiber tensile test setup in accordance with ASTM D3822-01 (2017)

Test acquisition was controlled by dedicated software, yielding load–deformation curves for each filament. The initial portion of each curve was approximately linear, corresponding to the elastic regime, in which the fiber recovers its original length upon unloading. The initial linear portion of each curve corresponds to the elastic regime. Although this region can be used to estimate the intrinsic Young's modulus, in the present work the single-fiber tensile tests were primarily conducted to determine the strain at break as a function of gauge length. Because the likelihood of critical flaws increases with gauge length, deformation metrics were targeted at the shortest practical lengths. To estimate the maximum theoretical strain at failure for an ideal fiber, natural fibers were tested at gauge lengths of 1", ¾", ½", and ¼", and the resulting strain-at-break data were extrapolated to a 0 mm intercept (Fig. 3). This parameter was subsequently extrapolated to a zero-length condition to estimate the theoretical maximum strain at break, which was used as input for the MFA calculation. Although fiber diameter measurements were available, they were not required for the strain-at-break extrapolation procedure.

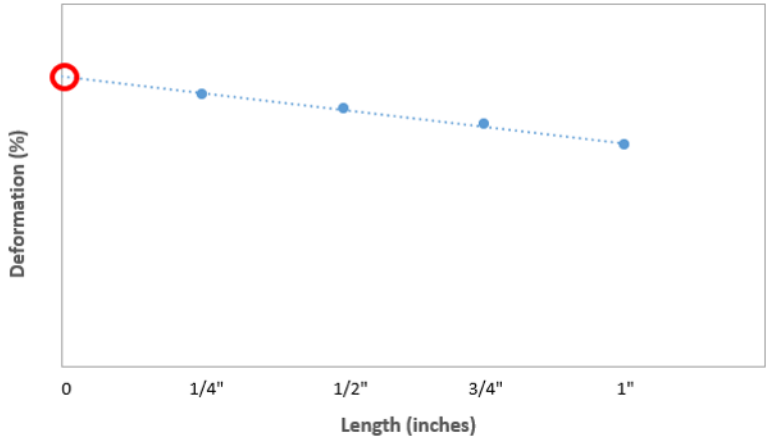

Fig. 3. Dependence of strain at break on single fiber length

MFA-based Models

Quadratic relationships between elongation and microfibril angle (MFA) have been proposed in the literature (Isik *et al.* 2008). However, these formulations generally show only a weak link between these two variables, and the MFA values back-calculated from these formulae have been reported as physically implausible (Barnett and Bonham 2004). To address these limitations, the authors derived an alternative expression by combining their experimental results with literature datasets from multiple natural-fiber filaments. Plotting MFA against strain at break produced a second-order trend, leading to a quadratic fit that remains consistent with earlier reports (De Souza *et al.* 2022).

Flexural Modulus Evaluation

The flexural modulus of the composite materials was evaluated by three-point bending tests in accordance with ASTM D790-17 (2026). Test specimens were manufactured following the same standard, with nominal dimensions of 127 × 12.7 × 3.2 mm. A minimum of five specimens was tested for each composite formulation. Flexural measurements were carried out using an Instron® 1122 universal testing machine (Metrotec, S.A., Barcelona, Spain) equipped with a 5000 N load cell. Tests were performed at a strain rate of 0.10 mm/mm/min and a support span of 52.6 mm.

Composites with HS contents between 20 and 50 wt.% were prepared using a fixed MAPP content of 4 wt.%. This content was selected based on previous work (Tarrés *et al.* 2019), where it was identified as near-optimal for interfacial performance in the same PP–henequen system. However, no sensitivity analysis of MAPP content was conducted within the present study, and therefore its independent contribution to the mechanical response cannot be isolated.

In addition, neat PP specimens were tested under identical conditions to provide a reference baseline. Results are reported as mean values ± standard deviation.

Correlation between Flexural Modulus and Cel, CI and MFA

Based on previous work (Seculi *et al.* 2025), a predictive linear equation was derived to estimate the intrinsic flexural modulus. This methodology involves a regression analysis that correlates the modulus with a combined factor of cellulose content, crystallinity index (CI), and MFA. The dataset used to generate this model comprises both proprietary experimental results and data harvested from literature. The equation was defined as,

$$\delta = Cel \cdot CI/MFA \quad (2)$$

Due to morphological constraints, specifically fiber length, this correlation was not verified for wood-based or recycled fibers.

Micromechanics Models

Modified rules of mixtures

Short fiber composites were modeled according to a modified rule of mixtures (mRoM) to predict their mechanical properties (Fukuda and Chou 1982; Korabel'nikov and Rashkovan 2006), as given by Eq. 3,

$$E_f^C = \eta_e \cdot E_f^F \cdot V^F + (1 - V^F) \cdot E_f^M \quad (3)$$

where E_t^C, E_t^F and E_t^M represent the flexural moduli of the composite, reinforcement, and matrix, respectively. The volume fraction of the reinforcement is V^F, and η_e is an efficiency factor. The efficiency factor should be 1 in an ideal composite, so the closer it is to 1, the higher will be the contribution of the reinforcements to the flexural modulus of the composite. This efficiency factor is the product of a length efficiency factor (η_l) by an orientation factor (η_o), being $\eta_e = \eta_l \cdot \eta_o$.

A Fiber Flexural Modulus Factor (FFMF) is described as the slope of the regression line derived from the contributions of the fibers at different contents (Espinach *et al.* 2013), shown in Eq. 4.

$$FFMF = \frac{E_f^c - (1 - V^F) \cdot E_f^M}{V^F} = \eta_e \cdot E_f^F \quad (4)$$

The modified rule of mixtures introduces two unknowns, E_f^F and η_e, which require additional modeling to resolve.

Hirsch's model

The intrinsic properties of the fiber were determined by the use of Hirsch's model, following successful precedents in the literature (Hirsch 1962; López *et al.* 2011; Espinach *et al.* 2015):

$$E_f^C = \beta \cdot \left(E_f^F \cdot V^F + E_f^M \cdot (1 - V^F) \right) + (1 - \beta) \cdot \frac{E_f^F \cdot E_f^M}{E_f^M \cdot V^F + E_f^F \cdot (1 - V^F)} \quad (5)$$

where β is an efficiency factor related to orientation and the load transfer between fibers and the matrix. For short semi-aligned fibers reinforced composites, β is typically 0.4 (Kalaprasad *et al.* 1997). When E_f^F is defined, η_e can be obtained by using the mRoM (Eq. 4).

Tsai and Pagano model and Halpin Tsai equations

The Tsai and Pagano model, along with the Halpin and Tsai equations (Tsai *et al.* 1968; Kalaprasad *et al.* 1997; Raju and Shanmugaraja 2021), predict the intrinsic flexural modulus of the fiber from experimental data. The Tsai and Pagano model is formulated as,

$$E_f^C = \frac{3}{8} \cdot E^{11} + \frac{5}{8} \cdot E^{22} \quad (6)$$

where E^{11} and E^{22} are the longitudinal flexural modulus and the transversal flexural modulus, respectively. The Halpin and Tsai for these moduli are,

$$E^{11} = \frac{1+2\cdot\left(\frac{l^F}{d^F}\right)\cdot\eta_l\cdot V^F}{1-\eta_l\cdot V^F}\cdot E_f^M \quad (7)$$

$$E^{22} = \frac{1+2\cdot\eta_t\cdot V^F}{1-\eta_t\cdot V^F}\cdot E_f^M \quad (8)$$

where the parameters η_l and η_t are defined as follows,

$$\eta_l = \frac{\left(\frac{E_f^F}{E_f^M}\right)-1}{\left(\frac{E_f^F}{E_f^M}\right)+2\cdot\left(\frac{l^F}{d^F}\right)} \quad (9)$$

$$\eta_t = \frac{\left(\frac{E_f^F}{E_f^M}\right)-1}{\left(\frac{E_f^F}{E_f^M}\right)+2} \quad (10)$$

where d^F is the reinforcements' mean diameter.

Nielsen's modification

The Nielsen model refines the Halpin and Tsai equations by introducing a new parameter (ψ), as follows:

$$E^{11} = \frac{1+2\cdot\left(\frac{l^F}{d^F}\right)\cdot\eta_l\cdot V^F}{1-\psi\cdot\eta_l\cdot V^F}\cdot E_f^M \quad (11)$$

$$E^{22} = \frac{1+2\cdot\eta_t\cdot V^F}{1-\psi\cdot\eta_t\cdot V^F}\cdot E_f^M \quad (12)$$

where ψ is defined by:

$$\psi = 1 + \frac{(1-\phi_{max})}{\phi_{max}^2}\cdot V^F \quad (13)$$

For a square distribution of fibers, ϕ_{max} is typically 0.785 according to the literature (Sudheer *et al.* 2015; Alhijazi *et al.* 2021).

RESULTS AND DISCUSSION

Fiber Content Effect on Flexural Properties

PP-based composites containing 20 to 50 weight percent (wt.%) of HS were synthesized and evaluated. Table 1 presents a comparison between the fiber volume fraction (V^F) and the flexural modulus (E_f^C) of the HS-reinforced PP composites. A positive correlation was observed between the HS content and the flexural modulus of the composites. The highest flexural modulus recorded was 3.75 GPa, which was achieved with the incorporation of 50 wt.% HS. This represents a 3.3-fold improvement compared to the unreinforced PP matrix. Composites with HS content exceeding 50 wt.% were not investigated due to increased attrition phenomena, which significantly reduced the mean length of the fibers, thereby diminishing their reinforcing and stiffening capabilities (Pickering *et al.* 2007). Furthermore, above 50 wt.% fiber content, natural fiber–PP composites typically exhibit a pronounced increase in melt viscosity and a corresponding

drop in melt flow index, which severely hinders mold filling and renders injection molding impractical under standard processing conditions (Maurya and Manik 2023).

Table 1. Flexural Modulus of PP Composites Reinforced with HS, with a 4% Content of MAPP

Samples	V^F	E_f^C (GPa)	ε_f^c (%)	E_f^F (GPa)
PP	0	1.15 ± 0.02	6.6 ± 0.03	
PP + 20% Henequen + 4%MAPP	0.133	2.05 ± 0.11	5.0 ± 0.05	16.3
PP + 30% Henequen + 4%MAPP	0.208	2.65 ± 0.15	4.3 ± 0.07	17.2
PP + 40% Henequen + 4%MAPP	0.290	3.15 ± 0.12	2.8 ± 0.16	16.2
PP + 50% Henequen + 4%MAPP	0.379	3.75 ± 0.18	2.1 ± 0.04	15.8

In addition to fiber attrition, very high fiber loadings typically limit matrix availability for full wetting and impregnation; thus, beyond ~50 wt.% the system may approach a processing/packing threshold where agglomeration and fiber–fiber contacts begin to penalize the effective stiffness despite the higher V^F (Gassan and Bledzki 1998). These findings align with existing literature on natural fiber-reinforced composites, which predict an increase in stiffness and a reduction in deformation capacity as fiber content rises (Ku *et al.* 2011). This indicates an increase in brittleness and hardness of the composites. Consistently, the fracture mode is observed to transition from ductile matrix-dominated failure in neat PP to a more brittle, fiber-dominated response in the composites, with a gradual substitution of interfacial debonding/pull-out by fiber breakage as V^F increases (Bourmaud and Baley 2009).

The flexural modulus exhibited a linear relationship with the fiber volume fraction V^F, described by the regression equation $E_f^C = 6.89V^F + 1.16$, with a coefficient of determination (R^2) of 0.99. This linear behavior suggests effective dispersion of the reinforcement fibers during compounding (Joseph *et al.* 1993). The near-unity linearity is also consistent with rule-of-mixtures expectations for well-coupled, short-fiber thermoplastic composites, further supporting that the interphase created by MAPP is contributing to efficient load transfer rather than being the limiting factor (Doan *et al.* 2006). As anticipated, strain at break is negatively correlated with fiber volume fractions; higher volume fractions result in an increased presence of a stiffer and more brittle phase within the composite. Consequently, the fracture mechanism transitions from ductile in the matrix to brittle in the composites. The monotonic decline of ε_f^c without evidence of a plateau suggests that interfacial debonding does not dominate; instead, the reinforcement network increasingly constrains plastic deformation of PP, which explains the marked drop from 6.6% (neat PP) to 2.1% at V^F = 0.379.

Intrinsic flexural modulus estimations obtained *via* the Hirsch model indicate that the addition of fiber did not significantly impact this property, as expected for a fundamental property, yielding an average value of 16.4±0.6 GPa. Since micromechanical models estimate the effective contribution of the reinforcement within the composite rather than the actual intrinsic modulus of isolated fibers, the obtained values should be interpreted as lower-bound estimations of the intrinsic flexural modulus. Consequently, the real intrinsic modulus of henequen fibers is expected to be equal to or higher than the values predicted by the models. Previous studies have shown that the flexural modulus of natural fiber composites had the same behavior (Herrera-Franco and Valadez-González 2004).

The slight reduction of the apparent fiber modulus at the highest V^F value (from ~17.2 to ~15.8 GPa) can be rationalized by incipient fiber crowding and

imperfect impregnation at very high loadings, which would marginally reduce the effective efficiency factor even under adequate chemical coupling (Fu *et al.* 2000; Pickering *et al.* 2007).

Fiber Contribution to Flexural Modulus

The linear relationship between the composites Young's modulus and fiber content permits the use of linear models such as a modified Rule of Mixtures (mRoM). This model is employed to determine the contribution of the reinforcement to the flexural modulus of the composite materials as function of the fiber content. Figure 4 illustrates the contribution of the HS to the flexural modulus of the composites and provides the linear regression lines, where the slope represents the fiber Flexural Modulus factor (FFMF) (y=8.0677x with a R^2=0.9998). The high linearity confirms a consistent stiffening effect of the fibers within the studied fiber content range and validates the applicability of the mRoM for these systems The FFMF is an effective indicator of the stiffening efficiency of fibers under bending loads and is commonly employed for comparative purposes among different fiber–matrix systems.

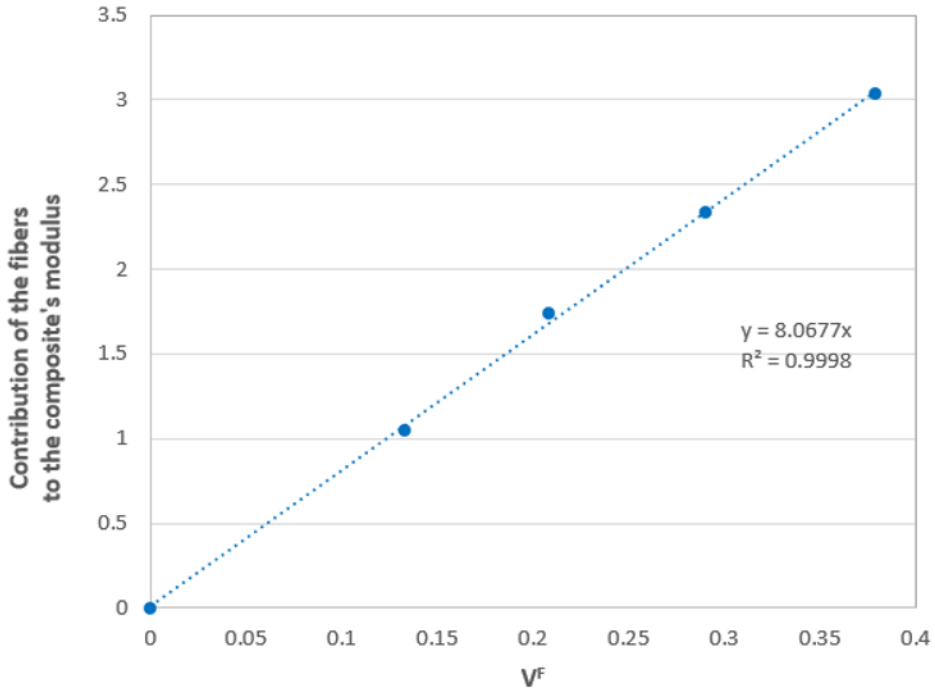

Fig. 4. HS contribution to the flexural modulus against fiber volume fraction

The FFMF of HS as PP reinforcement was determined to be 8.0677, which is lower than the Fiber Tensile Modulus Factor (FTMF) of 14.426 obtained for the same reinforcements in previous research (Espinach *et al.* 2022). This difference is commonly attributed to the non-uniform stress distribution inherent to flexural loading, where only a fraction of the fibers reaches maximum stress, resulting in a reduced effective contribution compared to uniaxial tensile loading.

The obtained FFMF value can be compared with other polypropylene-based composites reinforced with different materials reported in the literature. The FFMF of cotton fiber uncoupled and coupled reinforced PP composites were 9.43 and 8.71, respectively (Serra *et al.* 2019), and the FFMF of hemp fiber-reinforced PP was 8 (Hao *et*

al. 2020). These results indicate that HS provides stiffening efficiency under flexural loading like that of cotton and hemp fibers, producing comparable increases in composite flexural modulus for equivalent fiber volume fractions. This reinforces the suitability of HS as an effective natural reinforcement for PP composites when stiffness-driven design requirements are considered.

Determination of the Maximum Strain at Break of Henequen

The theoretical maximum strain at break of the Henequen was determined through extrapolation from Fig. 5, taking into consideration that the maximum value is found in the value closest to the length value 0 mm.

The value obtained by extrapolating the regression line graphically expressed in Fig. 5 is 8%. This extrapolated strain at break ($\varepsilon = 8\%$) represents the idealized deformation of an "infinitely short" or defect-free segment of the fiber, *i.e.*, the theoretical upper limit before the influence of gauge-length-dependent flaw activation. The decreasing trend of strain with increasing fiber length is fully consistent with Weibull statistics, where longer fibers have a higher probability of containing critical flaws, thus lowering their effective tensile deformation capacity (Harikrishnan *et al.* 2018). The linear degradation observed here (≈ –0.46 % per ¼″) suggests a uniform flaw distribution along the fiber, indicating that the structure of henequen bundles behaves mechanically as a quasi-brittle, defect-controlled natural fiber.

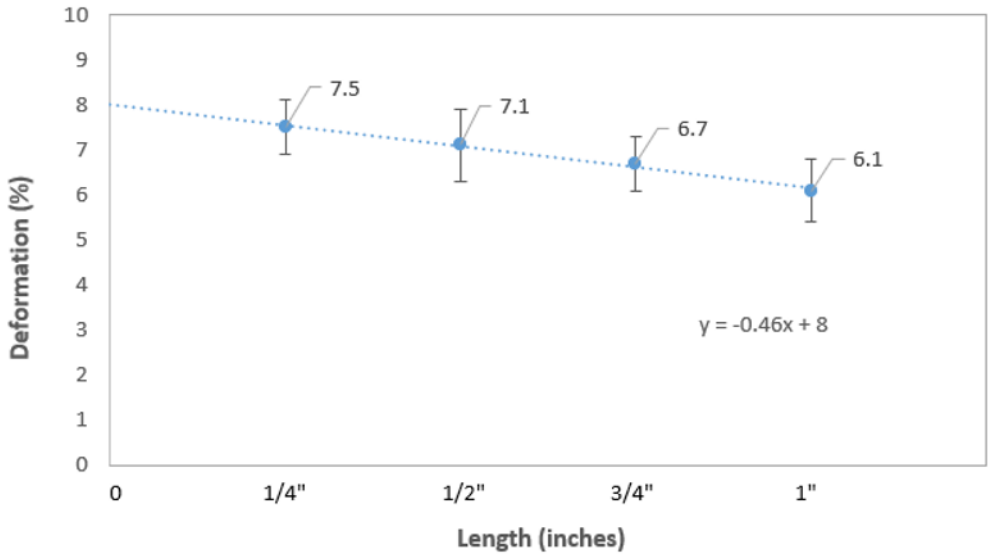

Fig. 5. Graphical representation of the strain at break versus single henequen fiber length

MFA Definition

In a previous work, a quadratic expression was defined to obtain the MFA of a natural fiber by introducing the ε of the fiber (Seculi *et al.* 2025), which was based on the quadratic expression found by Satyanarayama (Satyanarayana *et al.* 1982). This modified Satyanarayana equation allows for determining the MFA of the Henequen by introducing ε for a length equal to 0 mm, and is represented as follows:

$$MFA = -7.3832 + 4.4838\varepsilon - \frac{9.19}{100}\varepsilon^2 \quad (14)$$

The value obtained from this equation was MFA = 22.8°.

This MFA value (≈23°) is characteristic of moderately stiff lignocellulosic fibers and is fully compatible with the 8% intrinsic strain previously estimated. A lower MFA would typically yield higher stiffness and reduced strain-at-break, whereas a higher MFA (>30°) would shift the fiber towards a more extensible but less stiff profile (Königsberger *et al.* 2023). The internal consistency between ε = 8% and MFA ≈ 23° therefore strongly suggests that the molecular orientation of the cellulose microfibrils in henequen is optimized for a balanced ductile–stiff mechanical profile, characteristic of hard fibers used in cordage and composites applications (Abraham and Elbaum 2013).

Moreover, the MFA obtained aligns with the typical range reported for Agave fibers (≈18–25°) (Gebretsadik *et al.* 2023), which supports the reliability of the interpolation–extrapolation method employed to derive ε (0 mm). The smooth curvature of the Satyanarayana equation in this zone also indicates that the MFA result is not particularly sensitive to small errors in extrapolated strain, reinforcing the robustness of the calculation.

Relation between CI, %Cel, and MFA

Once the MFA of Henequen is defined, authors proceeded to establish the value of the relation between CI, %Cel, and MFA. This correlation was resolved in a previous work (Alonso-Montemayor *et al.* 2023), where it was expressed with Eq. 2.

The value of the content of cellulose of henequen was determined in a prior study (Tarrés *et al.* 2019), with % Cel=68.1. The crystallinity index of the fibers was determined by X-ray diffraction (XRD). Using this approach, a crystallinity index of 0.57 was obtained. Introducing these values into the equation, a value of δ=1.72 was determined. This value provides a meaningful integrative metric of fiber quality by condensing structural (CI), chemical (%Cel), and microstructural (MFA) parameters into a single descriptor. A relatively high δ is consistent with fibers presenting high cellulose content, significant crystalline fraction, and low-to-moderate MFA, all three of which are known contributors to reinforcing efficiency in polymer composites (Königsberger *et al.* 2023).

A δ value around 1.7 is particularly notable because it aligns with the mechanical performance previously calculated ($E_f^F \approx$ 16 to 17 GPa in composites), confirming that the intrinsic structural attributes of henequen, especially its crystallinity and microfibrillar orientation, are fully coherent with the stiffening observed experimentally.

Finally, δ acts as a predictor of composite performance: higher δ typically correlates with higher modulus and lower deformation in the composite phase. The fact that δ, MFA, and ε were mutually consistent here suggests that HS possess an advantageous combination of crystallinity and orientation that explains both the linear reinforcement behavior observed in PP composites and the strong dependence of failure strain on fiber length.

Prediction of the Composite Flexural Modulus

Once the intrinsic flexural modulus of the henequen was established, the authors used the Hirsch model to predict the flexural modulus of the composite comprising 20 to 50 wt.% of HS. The values are shown in Table 2. For the subsequent Hirsch predictions, a value of 16.2 GPa was selected as a conservative estimate within the range obtained from the micromechanical analysis.

Table 2. Flexural Modulus of PP Composites Reinforced with HS, with a E_f^F=16.2 GPa Calculated by Hirsch Model

Samples	V^F	E_f^C (GPa)	E_f^C (GPa)-Exp
PP	0	1.15 ± 0.02	1.15 ± 0.02
PP + 20% Henequen	0.133	2.048	2.05 ± 0.11
PP + 30% Henequen	0.208	2.567	2.65 ± 0.15
PP+ 40% Henequen	0.290	3.150	3.15 ± 0.12
PP + 50% Henequen	0.379	3.807	3.75 ± 0.18

When comparing the experimentally obtained values with those predicted by the model, the results demonstrate a high degree of concordance, with only minimal significant variations. This indicates that the prediction model is robust and reliable for determining the flexural modulus of a composite material based on the known composition of the natural fiber (Khan *et al.* 2025).

Furthermore, the close match between predicted and experimental moduli strongly suggests that the intrinsic fiber stiffness used as input in the Hirsch model (E_f^F =16.2 GPa) is representative of the real stiffening ability of HS within the PP matrix. The highest deviation (3%) appears at V^F = 0.208 to 0.379, which is within the typical scatter of natural-fiber reinforced composites and consistent with small variations in packing, fiber–fiber interactions, or local orientation effects during processing (Gholampour and Ozbakkaloglu 2020).

It is also relevant to note that the Hirsch model successfully captured the transition from matrix-dominated behavior at low V^F to fiber-dominated behavior at higher V^F. The slope of the predicted curve increased progressively with V^F, mirroring the experimental linear trend and reinforcing the conclusion that the mechanical behavior of PP–HS composites is governed largely by the fiber modulus and its volume fraction.

Additionally, the fact that the predicted modulus at V^F = 0.379 (3.807 GPa) slightly exceeded the experimental value (3.75 GPa) is physically meaningful: at high fiber loadings, processing-induced defects such as incomplete wetting, small fiber agglomerates and reduced matrix continuity can marginally decrease the experimental stiffness relative to the idealized model (Alhijazi *et al.* 2020). This behavior is common in natural fibers due to lumen collapse, surface roughness variability, and fiber length attrition during compounding. The smoothness of the model–experiment discrepancy curve indicates that these microstructural imperfections do not drastically affect the global mechanical response, reinforcing the robustness of the micromechanical assumptions used in the calculation.

Determination of Flexural Modulus Range of the Composite

Considering that the most common values for the modulus efficiency factor (η_e) ranges between 0.45 and 0.55, the flexural modulus of the composite material was calculated using different contents of HS ranging from 20 to 50 wt.%. Calculations were performed using both efficiency factor values to create what can be referred to as a common value range, within which the flexural modulus is expected to lie. These values are presented in Table 3.

Table 3. Flexural Modulus of the Composites with η_e=0.45 and η_e=0.55

Samples	V^F	E_f^c (GPa)	E_f^c (GPa)
PP	0	1.15 ± 0.02	
PP + 20% Henequen	0.133	1.96662	2.18208
PP + 30% Henequen	0.208	2.42712	2.76408
PP+ 40% Henequen	0.290	2.9306	3.4004
PP + 50% Henequen	0.379	3.47706	4.09104

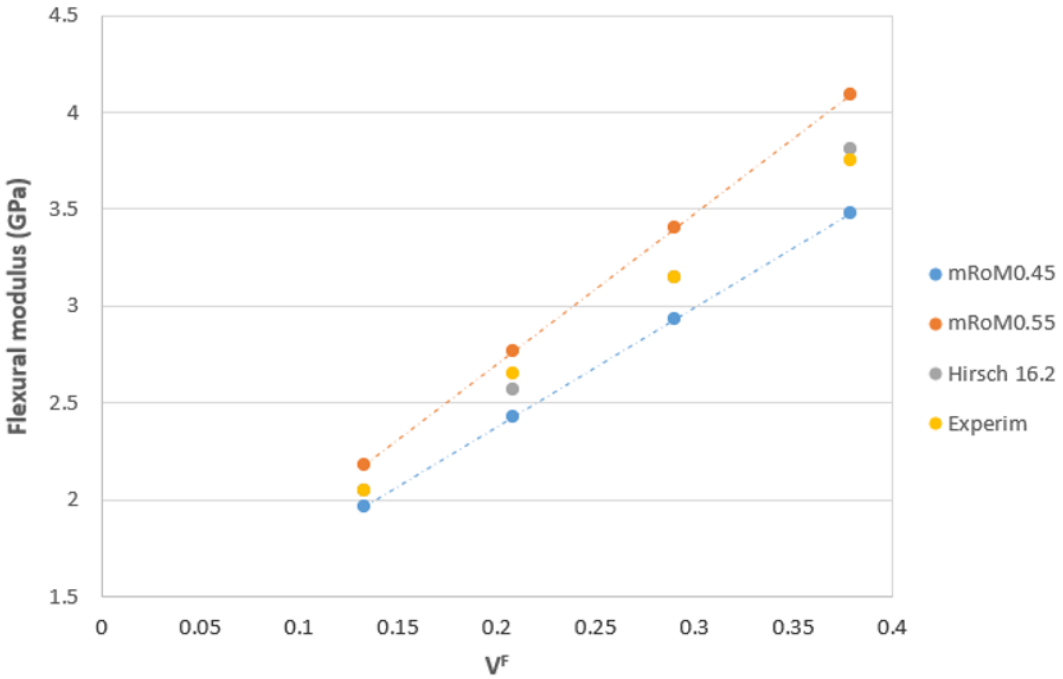

Fig. 6. Range of values of the flexural modulus of the composite by the four different methods explored

In Fig. 6, the flexural modulus values calculated using the modified rule of mixtures (mRoM) are shown, with η_e values of 0.45 and 0.55 determining the expected minimum and maximum values (Atmakuri *et al.* 2025). The experimentally obtained values, as well as those obtained with the prediction model developed by the authors, fell within this range.

This agreement demonstrates that the mRoM envelopes generated with η_e = 0.45 and η_e = 0.55 effectively bracketed the real mechanical response of the PP–HS composite system. The lower bound (η_e = 0.45) corresponds to conditions where fiber alignment, effective aspect ratio and spatial distribution are less favorable, whereas the upper bound (η_e = 0.55) reflects morphologies characterized by longer, better oriented fibers and reduced fiber–fiber interactions. That the experimental data fell consistently between these two limits confirms that the micromechanical behavior of the composite can be quantitatively described through classical short-fiber models without invoking additional correction factors (Chahar *et al.* 2025).

The proximity of the experimental results to the upper η_e = 0.55 boundary at low V^F indicates that reinforcement efficiency is maximized at low fiber contents, where dispersion is more uniform and geometric constraints such as fiber crowding and misalignment are minimized. However, at higher V^F (≥0.29), the experimental values approach the mid-range between both curves, which is consistent with the onset of fiber–fiber contact, partial fiber misalignment, and reduced matrix continuity. All these

phenomena naturally decrease the effective efficiency factor without contradicting the fundamental reinforcement trend (Ramachandran *et al.* 2025).

The fact that Hirsch-equation predicted values that lie inside the mRoM envelope further validates the fiber modulus used in both models and confirms that the composite behaviour is strongly fiber-dominated. The convergence of four independent prediction paths (η_e=0.45, η_e=0.55, Hirsch model, and experimental measurements) is a strong indicator that the mechanical performance of this PP–HS system is internally consistent and structurally well understood.

The widening of the modulus range with increasing V^F (from a spread of 0.22 GPa at V^F=0.133 to 0.61 GPa at V^F=0.379) highlights the growing sensitivity of composite stiffness to fiber orientation, packing density, and dispersion quality at higher fiber loadings. This behaviour agrees with micromechanical consideration, since a higher fiber dominance amplifies the effect of slight microstructural imperfections on stiffness, resulting in a greater dispersion of η_e at high V^F.

Nonetheless, the experimental modulus remained well centered between the two prediction curves, showing that even at 50 wt.% HS the PP–MAPP system maintained sufficient impregnation and coupling efficiency to avoid a significant drop in reinforcement efficiency. This reinforces the conclusion that maximum stiffness values estimated by the model represent a realistic upper bound rather than an unattainable theoretical limit.

Comparison of the Composite Flexural Modulus using Different Micromechanical Models

The authors employed three micromechanical models to determine and assess the intrinsic flexural modulus of HS: Hirsch, Tsai-Pagano (T-P), and T-P with the modification proposed by Nielsen (Table 4). The mean weighted lengths of HS extracted from the 20 to 50 wt.% composites were 784.2±12.3, 741.9±5.9, 708.1±17.2, and 674.3±7.2 μm, respectively. The mean diameters for these fibers were 25.6±0.1, 25.3±0.2, 25.4±0.2, and 25.5±0.1 μm, respectively. These values correspond to measurements previously reported (Espinach *et al.* 2022), obtained from the same set of composite specimens analyzed in the present study. These properties were utilized to apply the Tsai–Pagano model and its Nielsen-modified version.

Table 4. E_f^F values of HS Estimated Using the Models of Hirsch, Tsai-Pagano, and Nielsen

Samples	V^F	E_f^C Hirsch (GPa)	E_f^C T-P (GPa)	E_f^C Nielsen (GPa)
PP + 20% Henequen + 4%MAPP	0.133	16.29	16.36	16.40
PP + 30% Henequen + 4%MAPP	0.208	17.21	17.22	17.16
PP+ 40% Henequen + 4%MAPP	0.290	16.65	15.99	15.91
PP + 50% Henequen + 4%MAPP	0.379	15.81	14.45	14.34
Mean value		16.49 ± 0.59	16.01 ± 1.16	15.94 ± 1.19

The mean values obtained from the three models were similar, especially when considering the range of values influenced by their standard deviations. The highest mean value was obtained using the Hirsch model, while the lowest was obtained using the T-P Nielsen's modification model. Figure 7 illustrates that all three models exhibit similar behavior with increasing reinforcement content. The authors suggest that these methods provide a lower bound for the intrinsic flexural modulus (Park *et al.* 2010; French and

Santiago Cintrón 2013), implying that the actual intrinsic modulus will be equal to or greater than the values presented in Table 4.

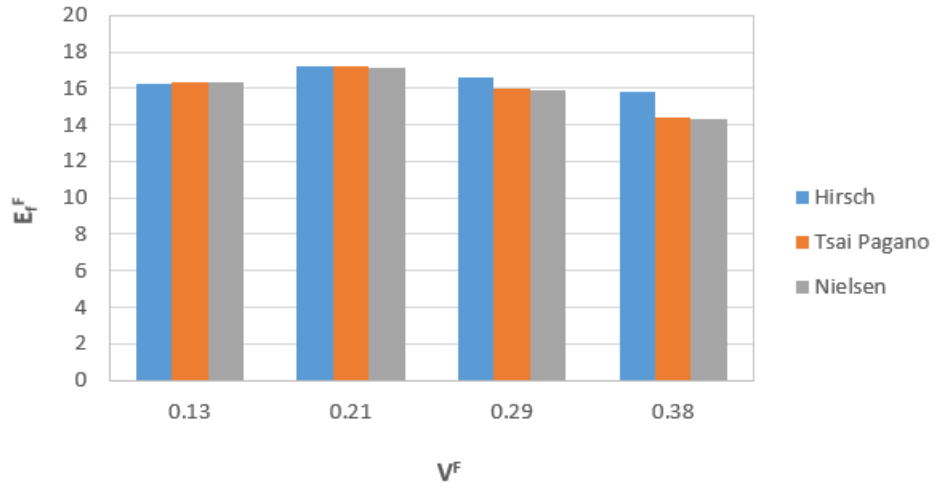

Fig. 7. Intrinsic moduli representation of HS obtained by using three micromechanics models

The progressive decrease in the intrinsic modulus estimated by all models as V^F increases (particularly evident between 0.208 and 0.379) is physically meaningful. At high fiber volume fractions, fiber–fiber contact increases and matrix availability decreases. Consequently, complete impregnation of the reinforcement becomes more difficult and wetting efficiency may decrease, producing small reductions in the effective contribution of individual fibers to the global stiffness (Serra-Parareda *et al.* 2021; Khan *et al.* 2025). Because the intrinsic modulus in these models is back-calculated from composite behavior, any loss of reinforcement efficiency (due to misalignment, uneven dispersion or matrix starvation) is reflected as a slight apparent decrease in E_f^F. This explains why the highest calculated intrinsic moduli occur at lower V^F, where fibers are more isolated and fully engaged, and why values slowly drop at higher fiber loadings.

The fact that the Hirsch model consistently produces the highest E_f^F values agrees with its theoretical basis: Hirsch combines "parallel" and "series" models and tends to return results closer to the upper performance limit for partially aligned fiber systems. Tsai-Pagano, on the other hand, explicitly accounts for orientation effects through stiffness matrices and therefore predicts slightly lower intrinsic fiber moduli when moderate misalignment is present, a realistic scenario in natural-fiber composites (French and Santiago Cintrón 2013).

Nielsen's modification further reduces the predicted E_f^F because it incorporates packing and porosity effects. In natural fibers, lumen presence and surface irregularities decrease the effective stiffness contribution of each fiber in the composite; thus, Nielsen's correction naturally results in the lowest modulus values (Park *et al.* 2010). This provides a more conservative estimate, which is particularly suitable when fibers exhibit significant variability in morphology.

Despite these conceptual differences, the close convergence of all three models (within a range of 0.5 to 1 GPa) indicates that the intrinsic modulus of henequen is a reproducible and reliable material parameter rather than a model-dependent artifact. This convergence is remarkable, considering the heterogeneity of natural fibers. This strongly

suggests that micromechanical predictions are not significantly affected by local imperfections (Khan *et al.* 2025) or minor measurement uncertainties in fiber length or diameter.

Furthermore, the decreasing trend of E_f^F with increasing V^F supports the hypothesis that intrinsic fiber properties remain constant, and that the observed variations arise from composite microstructural factors rather than true fiber stiffness changes. This is consistent with the mechanical behavior previously reported for henequen, where fiber interactions, not intrinsic fiber damage, govern changes in composite modulus.

Finally, because the Tsai–Pagano and Nielsen approaches explicitly account for fiber orientation effects, packing constraints and possible fiber–matrix slip, they tend to underestimate stiffness in systems with partial alignment or non-ideal interfaces, and can therefore be legitimately interpreted as lower-bound estimates. Likewise, in the present work the Hirsch model was applied using a fixed β value (β = 0.4), commonly associated with randomly oriented or semi-aligned short-fiber composites. Under these conservative assumptions, Hirsch predictions also represent a lower-bound estimate of the intrinsic fiber stiffness rather than an upper theoretical limit.

CONCLUSIONS

1. The mechanical characterization and micromechanical analysis performed in this work indicate that the polypropylene-henequen strands (PP–HS) composites behaved as a structurally coherent and internally consistent natural fiber composite, with a consistency between experimental data and theoretical predictions.
2. The intrinsic strain at break extrapolated for HS (ε ≈ 8%) was fully consistent with the microfibrillar angle obtained through the modified Satyanarayana model (MFA = 22.8°). This pairing confirms a molecular architecture typical of hard lignocellulosic fibers: moderately aligned microfibrils, significant crystalline contribution, and a balanced ductility–stiffness profile.
3. The structural indicator δ = 1.72, derived from CI, %Cel, and MFA, validated that henequen possesses the microstructural traits required for effective reinforcement in polymer matrices. The consistency between δ and the micromechanically extracted E_f^F (≈16–17 GPa) further supported the robustness of the intrinsic property estimations.
4. The flexural modulus of the composite increased linearly with fiber content (R^2 = 0.99), in agreement with efficient fiber dispersion and a well-defined transition from matrix-dominated to fiber-dominated behavior as V^F increases. The progressive reduction in strain at break was compatible with this transition.
5. The Micromechanical models (Hirsch, Tsai-Pagano, and Nielsen) provided consistent estimations of E_f^F. The slight divergence observed at high V^F was associated with increasing influence of fiber interactions, imperfect alignment and matrix availability, which affect the effective stiffness of the composite.
6. The Hirsch model showed strong concordance with experimental results and provided a reliable estimation of the intrinsic fiber modulus, while the mRoM using η_e=0.45-0.55 defined an accurate stiffness range within which both experimental data and model predictions consistently fell.

7. Overall, the combination of experimental testing, micromechanical modelling and microstructural interpretation indicates that HS are suitable as reinforcement in PP matrices and that the predict models used in this study describe the composite flexural behavior across the full range of fiber contents.

ACKNOWLEDGEMENTS

The authors acknowledge that no specific funding or additional support was received for this work.

Conflict of Interest

The authors declare no conflicts of interest.

Use of Generative AI

No generative AI tools were used in the preparation of the scientific content of this manuscript.

REFERENCES CITED

Abraham, Y., and Elbaum, R. (2013). "Quantification of microfibril angle in secondary cell walls at subcellular resolution by means of polarized light microscopy," *New Phytologist* 197(3), 1012-1019. https://doi.org/10.1111/nph.12070

Affdl, J. H., and Kardos, J. L. (1976). "The Halpin-Tsai equations: A review," *Polymer Engineering and Science* 16(5), 344-352. https://doi.org/10.1002/pen.760160512

Alhijazi, M., Safaei, B., Zeeshan, Q., and Asmael, M. (2021). "Modeling and simulation of the elastic properties of natural fiber-reinforced thermosets," *Polymer Composites* 42(7), 3508-3517. https://doi.org/10.1002/pc.26083

Alhijazi, M., Zeeshan, Q., Qin, Z., Safaei, B., and Asmael, M. (2020). "Finite element analysis of natural fibers composites: A review," *Nanotechnology Reviews* 9(1), 853-875. https://doi.org/10.1515/ntrev-2020-0069

Alonso-Montemayor, F. J., Espinach, F. X., Tarrés, Q., Alcalà, M., Delgado-Aguilar, M., and Mutjé, P. (2023). "The evolution of the intrinsic flexural strength of jute strands after a progressive delignification process and their contribution to the flexural strength of PLA-based biocomposites," *Polymers* 16(1), article 37. https://doi.org/10.3390/polym16010037

Anaya-Ramirez, R. C., Rios-Soberanis, C. R., and Herrera-Franco, P. J. (2022). "Effect of fiber surface treatments in HDPE-henequen short fiber-reinforced composites: Static characterization and fatigue," *Journal of Materials Science* 57(33), 15762-15776. https://doi.org/10.1007/s10853-022-07608-8

Anbupalani, M. S., Venkatachalam, C. D., and Rathanasamy, R. (2020). "Influence of coupling agent on altering the reinforcing efficiency of natural fibre-incorporated polymers – A review," *Journal of Reinforced Plastics and Composites* 39(13-14), 520-544. https://doi.org/10.1177/0731684420913170

ASTM D618-21 (2021). "Standard practice for conditioning plastics for testing," ASTM International, West Conshohocken, PA, USA.

ASTM D790-17 (2026). "Standard test methods for flexural properties of unreinforced and reinforced plastics and electrical insulating materials," ASTM International, West Conshohocken, PA, USA.

ASTM D3641-21 (2024). "Standard practice for injection molding test specimens of thermoplastic molding and extrusion materials," ASTM International, West Conshohocken, PA, USA.

ASTM D3822-01 (2017). "Standard test method for tensile properties of single textile fibers," ASTM International, West Conshohocken, PA, USA.

Atmakuri, A., Palevicius, A., and Janusas, G. (2025). "Numerical and experimental analysis of natural-fiber-reinforced hybrid polymer composites," in: *Fiber-Based Hybrid Composites for Engineering*, Springer Nature, Cham, Switzerland, pp. 83-103.

Barnett, J. R., and Bonham, V. A. (2004). "Cellulose microfibril angle in the cell wall of wood fibres," *Biological Reviews* 79(2), 461-472. https://doi.org/10.1017/S1464793103006377

Biagiotti, J., Puglia, D., and Kenny, J. M. (2004). "A review on natural fibre-based composites," *Journal of Natural Fibers* 1(2), 37-68. https://doi.org/10.1300/J395v01n02_03

Bourmaud, A., and Baley, C. (2009). "Rigidity analysis of polypropylene/vegetal fibre composites after recycling," *Polymer Degradation and Stability* 94(3), 297-305. https://doi.org/10.1016/j.polymdegradstab.2008.12.010

Çavuş, V., and Mengeloğlu, F. (2020). "Effect of wood particle size on selected properties of neat and recycled wood polypropylene composites," *BioResources* 15(2), 3427-3442. https://doi.org/10.15376/biores.15.2.3427-3442

Chahar, M., Kumar, R., Habeeb, A., Kumar Garg, R., and Punia, U. (2025). "Factors affecting flexural and impact strength of natural fiber reinforced polymer composites: A review," *Green Materials* 13(2), 76-91. https://doi.org/10.1680/jgrma.24.00108

Chichane, A., Boujmal, R., and El Barkany, A. (2023). "A comparative study of analytical and numerical models of mechanical properties of composites and hybrid composites reinforced with natural reinforcements," *Polymers and Polymer Composites* 31, article 09673911231172491. https://doi.org/10.1177/09673911231172491

Cho, D., Lee, H. S., Han, S. O., and Drzal, L. T. (2007). "Effects of E-beam treatment on the interfacial and mechanical properties of henequen/polypropylene composites," *Advanced Composite Materials* 16(4), 315-334. https://doi.org/10.1163/156855107782325178

Clyne, T. W., and Hull, D. (2019). *An Introduction to Composite Materials*, 3rd Ed., Cambridge University Press, Cambridge, UK. https://doi.org/10.1017/9781139170130

Cox, H. L. (1952). "The elasticity and strength of paper and other fibrous materials," *British Journal of Applied Physics* 3(3), 72-79. https://doi.org/10.1088/0508-3443/3/3/302

De Souza, N. C. M., Lima, J. T., and Soares, B. C. D. (2022). "Application of X-ray diffraction to assess the microfibril angle of green and dry *Eucalyptus grandis* wood," *Trees* 36(1), 191-197. https://doi.org/10.1007/s00468-021-02194-9

Doan, T.-T.-L., Gao, S.-L., and Mäder, E. (2006). "Jute/polypropylene composites I. Effect of matrix modification," *Composites Science and Technology* 66(7-8), 952-963. https://doi.org/10.1016/j.compscitech.2005.08.009

El-Sabbagh, A. (2014). "Effect of coupling agent on natural fibre in natural fibre/ polypropylene composites on mechanical and thermal behaviour," *Composites Part B: Engineering* 57, 126-135. https://doi.org/10.1016/j.compositesb.2013.09.047

Erana, L. A. (2024). "Mechanical characterization of sisal fiber reinforced PP composite panels," *Journal of Natural Fibers* 21(1), article 2385563. https://doi.org/10.1080/15440478.2024.2385563

Espinach, F. X., Delgado-Aguilar, M., Puig, J., Julian, F., Boufi, S., and Mutjé, P. (2015). "Flexural properties of fully biodegradable alpha-grass fibers reinforced starch-based thermoplastics," *Composites Part B: Engineering* 81, 98-106. https://doi.org/10.1016/j.compositesb.2015.07.004

Espinach, F. X., Julian, F., Alcalà, M., Vilaseca, F., Carrasco, F., and Mutjé, P. (2022). "Effective tensile strength estimation of natural fibers through micromechanical models: The case of henequen fiber reinforced-PP composites," *Polymers* 14(22), article 4890. https://doi.org/10.3390/polym14224890

Espinach, F. X., Julian, F., Verdaguer, N., Torres, Ll., Pelach, M. A., Vilaseca, F., and Mutjé, P. (2013). "Analysis of tensile and flexural modulus in hemp strands/ polypropylene composites," *Composites Part B: Engineering* 47, 339-343. https://doi.org/10.1016/j.compositesb.2012.11.021

French, A. D., and Santiago Cintrón, M. (2013). "Cellulose polymorphy, crystallite size, and the Segal Crystallinity Index," *Cellulose* 20(1), 583-588. https://doi.org/10.1007/s10570-012-9833-y

Fu, S.-Y., Lauke, B., Mäder, E., Yue, C.-Y., and Hu, X. (2000). "Tensile properties of short-glass-fiber- and short-carbon-fiber-reinforced polypropylene composites," *Composites Part A: Applied Science and Manufacturing* 31(10), 1117-1125. https://doi.org/10.1016/S1359-835X(00)00068-3

Fukuda, H., and Chou, T.-W. (1982). "A probabilistic theory of the strength of short-fibre composites with variable fibre length and orientation," *Journal of Materials Science* 17(4), 1003-1011. https://doi.org/10.1007/BF00543519

Gassan, J., and Bledzki, A. K. (1998). "Possibilities for improving the mechanical properties of jute/epoxy composites by alkali treatment of fibres," *Composites Science and Technology* 59(9), 1303-1309. https://doi.org/10.1016/S0266-3538(98)00169-9

Gebretsadik, T. T., Tesfay, A. H., Gebru, A. G., Assayehegn, E., Desta, Y. H., Gebremedhin, K. H., Gebrehiwet, H., and Teklemedhin, T. B. (2023). "Characterization and comparative insights on *Agave americana* and *Agave sisalana* leaf fibers for high-performance applications," *Journal of Natural Fibers* 20(2), article 2246648. https://doi.org/10.1080/15440478.2023.2246648

Geyer, R., Jambeck, J. R., and Law, K. L. (2017). "Production, use, and fate of all plastics ever made," *Science Advances* 3(7), article e1700782. https://doi.org/10.1126/sciadv.1700782

Gholampour, A., and Ozbakkaloglu, T. (2020). "A review of natural fiber composites: Properties, modification and processing techniques, characterization, applications," *Journal of Materials Science* 55(3), 829-892. https://doi.org/10.1007/s10853-019-03990-y

Hao, X., Zhou, H., Mu, B., Chen, L., Guo, Q., Yi, X., Sun, L., Wang, Q., and Ou, R. (2020). "Effects of fiber geometry and orientation distribution on the anisotropy of mechanical properties, creep behavior, and thermal expansion of natural fiber/HDPE composites," *Composites Part B: Engineering* 185, article 107778.

https://doi.org/10.1016/j.compositesb.2020.107778
Harikrishnan, R., Mohite, P. M., and Upadhyay, C. S. (2018). "Generalized Weibull model-based statistical tensile strength of carbon fibres," *Archive of Applied Mechanics* 88(9), 1617-1636. https://doi.org/10.1007/s00419-018-1391-9
Hariprasad, K., Ravichandran, K., Jayaseelan, V., and Muthuramalingam, T. (2020). "Acoustic and mechanical characterisation of polypropylene composites reinforced by natural fibres for automotive applications," *Journal of Materials Research and Technology* 9(6), 14029-14035. https://doi.org/10.1016/j.jmrt.2020.09.112
Herrera-Franco, P. J., and Valadez-González, A. (2004). "Mechanical properties of continuous natural fibre-reinforced polymer composites," *Composites Part A: Applied Science and Manufacturing* 35(3), 339-345. https://doi.org/10.1016/j.compositesa.2003.09.012
Hirsch, T. J. (1962). "Modulus of elasticity of concrete affected by elastic moduli of cement paste matrix and aggregate," *Journal of the American Concrete Institute* 59(3), 427-452.
Isik, F., Gumpertz, M., Li, B., Goldfarb, B., and Sun, X. (2008). "Analysis of cellulose microfibril angle using a linear mixed model in *Pinus taeda* clones," *Canadian Journal of Forest Research* 38(6), 1676-1689. https://doi.org/10.1139/X08-010
Joseph, K., Thomas, S., and Pavithran, C. (1993). "Dynamic mechanical properties of short sisal fiber reinforced low density polyethylene composites," *Journal of Reinforced Plastics and Composites* 12(2), 139-155. https://doi.org/10.1177/073168449301200203
Joseph, P. V., Rabello, M. S., Mattoso, L. H. C., Joseph, K., and Thomas, S. (2002). "Environmental effects on the degradation behaviour of sisal fibre reinforced polypropylene composites," *Composites Science and Technology* 62(10-11), 1357-1372. https://doi.org/10.1016/S0266-3538(02)00080-5
Kalaprasad, G., Joseph, K., Thomas, S., and Pavithran, C. (1997). "Theoretical modelling of tensile properties of short sisal fibre-reinforced low-density polyethylene composites," *Journal of Materials Science* 32(16), 4261-4267. https://doi.org/10.1023/A:1018651213311
Khan, T., Sebaey, T. A., Muthukumar, C., Rao, H. I., Shahroze, R. M., and Parthasarathy, V. (2025). "Prediction of the tensile properties of biocomposites: A review of micro-mechanical models," *Biomass Conversion and Biorefinery* 15(9), 13123-13141. https://doi.org/10.1007/s13399-024-06159-z
Königsberger, M., Lukacevic, M., and Füssl, J. (2023). "Multiscale micromechanics modeling of plant fibers: Upscaling of stiffness and elastic limits from cellulose nanofibrils to technical fibers," *Materials and Structures* 56(1), article 13. https://doi.org/10.1617/s11527-022-02097-2
Korabel'nikov, Yu. G., and Rashkovan, I. A. (2006). "Strength and mechanism of fracture of composites randomly reinforced with short carbon fibres," *Fibre Chemistry* 38(2), 142-146. https://doi.org/10.1007/s10692-006-0059-3
Ku, H., Wang, H., Pattarachaiyakoop, N., and Trada, M. (2011). "A review on the tensile properties of natural fiber reinforced polymer composites," *Composites Part B: Engineering* 42(4), 856-873. https://doi.org/10.1016/j.compositesb.2011.01.010
Lee, H. S., Cho, D., and Han, S. O. (2008). "Effect of natural fiber surface treatments on the interfacial and mechanical properties of henequen/polypropylene biocomposites," *Macromolecular Research* 16(5), 411-417. https://doi.org/10.1007/BF03218538
López, J. P., Méndez, J. A., El Mansouri, N.-E., Mutjé, P., and Vilaseca, F. (2011).

"Mean intrinsic tensile properties of stone groundwood fibers from softwood," *BioResources* 6(4), 5037-5049. https://doi.org/10.15376/biores.6.4.5037-5049

Sudheer, M., Pradyoth, K. R., and Somayaji, S. (2015). "Epoxy/glass: Elastic properties and fiber volume fraction," *American Journal of Materials Science* 5(3C), 11-15. https://doi.org/10.5923/c.materials.201502.03

Mansouri, A., Ben Nasr, J., and Ben Amar, M. (2024). "Biocomposites based on polypropylene and *Agave americana* L. fibers: Investigation on physical, thermal and mechanical properties," *Polymer Bulletin* 81(14), 12819-12840. https://doi.org/10.1007/s00289-024-05317-7

Maurya, A. K., and Manik, G. (2023). "Advances towards development of industrially relevant short natural fiber reinforced and hybridized polypropylene composites for various industrial applications: A review," *Journal of Polymer Research* 30(1), article 47. https://doi.org/10.1007/s10965-022-03413-8

Meys, R., Kätelhön, A., Bachmann, M., Winter, B., Zibunas, C., Suh, S., and Bardow, A. (2021). "Achieving net-zero greenhouse gas emission plastics by a circular carbon economy," *Science* 374(6563), 71-76. https://doi.org/10.1126/science.abg9853

Nairn, J. A., and Mendels, D. A. (2001). "On the use of planar shear-lag methods for stress-transfer analysis of multilayered composites," *Mechanics of Materials* 33(6), 335-362. https://doi.org/10.1016/S0167-6636(01)00056-4

OECD (2024). *Policy Scenarios for Eliminating Plastic Pollution by 2040*, OECD Publishing, Paris, France. https://doi.org/10.1787/76400890-en

Park, S., Baker, J. O., Himmel, M. E., Parilla, P. A., and Johnson, D. K. (2010). "Cellulose crystallinity index: Measurement techniques and their impact on interpreting cellulase performance," *Biotechnology for Biofuels* 3(1), article 10. https://doi.org/10.1186/1754-6834-3-10

Piao, Z., Agyei Boakye, A. A., and Yao, Y. (2024). "Environmental impacts of biodegradable microplastics," *Nature Chemical Engineering* 1(10), 661-669. https://doi.org/10.1038/s44286-024-00127-0

Pickering, K. L., Beckermann, G. W., Alam, S. N., and Foreman, N. J. (2007). "Optimising industrial hemp fibre for composites," *Composites Part A: Applied Science and Manufacturing* 38(2), 461-468. https://doi.org/10.1016/j.compositesa.2006.02.020

Plastics Europe (2024). *The Circular Economy for Plastics – A European Analysis*, Plastics Europe, Brussels, Belgium, (https://plasticseurope.org/knowledge-hub/the-circular-economy-for-plastics-a-european-analysis-2024/), Accessed June 9, 2026.

Raju, A., and Shanmugaraja, M. (2021). "Recent research in fiber reinforced composite materials: A review," *Materials Today: Proceedings* 46, 9291-9296. https://doi.org/10.1016/j.matpr.2020.02.141

Ramachandran, K., Khan, M., Tharuja Perera, R. A., and Daniel Jayaseelan, D. (2025). "Tensile and flexural behavior of synthetic and hybrid natural fiber composites for lightweight applications," *Polymer Composites* 46(S1), article e29781. https://doi.org/10.1002/pc.29781

Satyanarayana, K. G., Pillai, C. K. S., Sukumaran, K., Pillai, S. G. K., Rohatgi, P. K., and Vijayan, K. (1982). "Structure-property studies of fibres from various parts of the coconut tree," *Journal of Materials Science* 17(8), 2453-2462. https://doi.org/10.1007/BF00543857

Seculi, F., Espinach, F. X., Aguado, R. J., Mutjé, P., and Tarrés, Q. (2025). "Simple model to predict the intrinsic flexural modulus of abaca strands from crystallinity and

microfibril angle," *Polymer Composites* 46(5), 4558-4575. https://doi.org/10.1002/pc.29259

Segal, L., Creely, J. J., Martin, A. E., and Conrad, C. M. (1959). "An empirical method for estimating the degree of crystallinity of native cellulose using the X-ray diffractometer," *Text. Res. J.* 29, 786-794. https://doi.org/10.1177/004051755902901003

Serra, A., Tarrés, Q., Chamorro, M.-À., Soler, J., Mutjé, P., Espinach, F. X., and Vilaseca, F. (2019). "Modeling the stiffness of coupled and uncoupled recycled cotton fibers reinforced polypropylene composites," *Polymers* 11(10), article 1725. https://doi.org/10.3390/polym11101725

Serra-Parareda, F., Vilaseca, F., Aguado, R., Espinach, F. X., Tarrés, Q., and Delgado-Aguilar, M. (2021). "Effective Young's modulus estimation of natural fibers through micromechanical models: The case of henequen fibers reinforced-PP composites," *Polymers* 13(22), article 3947. https://doi.org/10.3390/polym13223947

Tarrés, Q., Vilaseca, F., Herrera-Franco, P. J., Espinach, F. X., Delgado-Aguilar, M., and Mutjé, P. (2019). "Interface and micromechanical characterization of tensile strength of bio-based composites from polypropylene and henequen strands," *Industrial Crops and Products* 132, 319-326. https://doi.org/10.1016/j.indcrop.2019.02.010

Tran, T. M. N., Pham, M. N., Lee, D.-W., and Song, J. (2025). "Enhanced mechanical and thermal properties of green PP composites reinforced with bio-hybrid fibers and agro-waste fillers," *Advanced Composites and Hybrid Materials* 8(2), article 224. https://doi.org/10.1007/s42114-025-01277-2

Tsai, S. W., Halpin, J. C., Pagano, N. J., and Schwartz, R. T. (1968). *Composite Materials Workshop*, Technomic Publishing Co., Stamford, CT, USA.

Zheng, J., and Suh, S. (2019). "Strategies to reduce the global carbon footprint of plastics," *Nature Climate Change* 9(5), 374-378. https://doi.org/10.1038/s41558-019-0459-z

Article submitted: June 7, 2026; Peer review completed: June 22, 2026; Revised version received and accepted: June 30, 2026; Published: July 14, 2026.
DOI: 10.15376/biores.21.3.8226-8248